Int J Clin Exp Pathol 2020;13(1):54-64
www.ijcep.com /ISSN:1936-2625/IJCEP0102825

Original Article

Mouse tail models of secondary lymphedema: fibrosis gradually worsens and is irreversible

Chenxiao Zhou[1], Wanchun Su[2], Haotian Han[1], Na Li[3], Gang Ma[4], Lei Cui[1,3]

Departments of [1]Plastic Surgery, [2]Lymph Surgery, [3]Central Laboratory, [4]Animal Laboratory, Beijing Shijitan Hospital, Capital Medical University, Beijing 100038, China

Received September 25, 2019; Accepted December 19, 2019; Epub January 1, 2020; Published January 15, 2020

Abstract: Although the mouse tail model of secondary lymphedema has been widely used in research, our knowledge regarding some of the characteristic changes in this model is lacking. Therefore, in the current study, we aimed to identify pathologic changes after surgery. Tail lymphedema was created in C57BL/6J mice by disconnecting both superficial and deep lymphatic vessels. The surgery resulted in chronic edema formation with the proliferation of subcutaneous adipose tissue, deposition of fibrotic tissue, and gradual increase in $CD4^+$ T lymphocyte infiltration. Furthermore, dramatic expansion and an increased number of lymphatic vessels were observed postoperatively. Lymphatic reflux was established at least 8 weeks after surgery, as evidenced by staining of the scar from the surgical excision. In addition, tissue fibrosis was irreversible, although $CD4^+$ T cell infiltration, tail swelling, and subcutaneous adipose hyperplasia were alleviated over time. We also show that necrosis could be effectively avoided by paying attention to several details in the modeling process. As animal models play a key role in exploring the pathophysiology of disease, our findings provide strong support for the study of lymphedema. The irreversibility of fibrosis suggests the importance of treating lymphedema by preventing fibrosis development.

Keywords: Mouse models, lymphedema, fibrosis

Introduction

Lymphedema is a condition of localized lymph fluid retention and tissue edema caused by an obstruction of lymphatic drainage, which includes both primary and secondary categories. Secondary lymphedema is more common and is most frequently observed after surgery and/or radiation therapy for cancer, infections (filariasis, cellulitis), lymph node dissection, and other causes of lymphatic obstruction [1]. Considering that lymphedema seriously affects quality of life in patients and is currently incurable, research on the pathology and treatment of lymphedema is in great demand. Animal models are an experimental basis for the study of disease, and for this reason, it is important to establish an effective animal model of lymphedema.

Regarding animal species, lymphedema models used in previous studies include rabbits, rats, dogs, pigs and others [2]. As inbred mouse populations have highly homozygous and stable genes (which facilitate the exchange of research results) and are easy to breed, they are widely used in experiments [2, 3]. According to the surgical site, mouse lymphedema models include tail [4], limb [5, 6], ear [7, 8], and abdominal wall models [9]. In addition to blocking lymphatic drainage by surgical approaches, transgenic mice can also be used to achieve modeling. Researchers have created mice that express the human diphtheria toxin receptor (DTR) on lymphatic endothelial cells (LECs), and the use of diphtheria toxin (DT) can ablate both capillary and collecting lymphatic vessels to induce lymphedema [10]. Due to limitations in obtaining transgenic mice, surgical approaches are still widely used to establish lymphedema models, with the mouse tail and limb models being the most common.

However, the tail and limb models have significant limitations. For example, the limb model requires adjuvant radiotherapy, which makes the modeling process cumbersome and time

consuming [5, 6]. For the tail model, the success rate is as low as 65% according to reports, and the tail readily becomes necrotic after surgery [3]. In addition, in these two models, the maximal swelling that occurs is noted shortly after surgery and resolves spontaneously over time [3, 10, 11].

Despite their various problems, tail and limb models are still the most widely used animal models, providing an important experimental basis for disease research. However, we still need to know more about these models to provide references for lymphedema research. Considering that the limb model requires adjuvant radiotherapy and that the surgical procedure is relatively cumbersome, the mouse tail model was selected in this study. This study was intended to improve the success rate of this mouse model through the mastery of details and to elucidate the characteristics of the model by testing postoperative pathologic changes to provide theoretical support for lymphedema research.

Materials and methods

Ethical approval

The animal experiments in this study were approved by the Animal Ethics Committee of Beijing Shijitan Hospital affiliated with Capital Medical University.

Lymphedema mouse tail model

Tail lymphedema was induced in 7 to 8-week-old C57BL/6J female mice (Vital River Laboratory, China) as previously described [3-6]. Considering that lymphedema affects females more often than males [12], we used only female mice for the study. Anesthesia was performed by intraperitoneally injecting 10% chloral hydrate (4 ml/1000 g). Briefly, a 2-mm wide circumferential full-thickness skin section was excised 2 cm distal to the tail base to remove superficial lymphatic vessels. The deep lymphatic vessels running parallel to the lateral tail vein were ligated and then ablated. Dissociation of the deep lymphatic vessels was carefully performed to reduce damage to the veins. The surgical incision was circumferentially wrapped with a 3M™ Tegaderm™ dressing to keep it moist, and the dressing was removed 24 hours later.

Edema evaluation

The diameter and volume of the tail in the lymphedema mouse model were measured using Vernier calipers and the immersion method, respectively. Measurements were performed every week for 9 weeks after the operation.

Analysis of lymphatic reflux

Lymphatic reflux was assessed with a noninvasive lymphatic vessel transport evaluation using indole cyanide green dye (ICG, 10 mg/ml, Meilunbio, China) or fluorescein isothiocyanate (FITC)-dextran (2000 kDa, 25 mg/ml, Sigma, USA).

Briefly, a controlled subcutaneous infusion of 10 μl of ICG (Meilunbio, China) was performed 1.5 cm proximal to the tail tip. An image of the region near the surgical excision margin was recorded 5 minutes later using a Xenogen IVIS Lumina II imaging system (Caliper Life Sciences) that was adapted for near-infrared spectroscopy (NIR) imaging.

For FITC-dextran detection, FITC-dextran was injected subcutaneously 1.5 cm proximal to the tail tip and visualized 15 minutes later using an Olympus MVX10 Macro View microscope (Japan). Fluorescence intensity was measured with ImageJ, and the ratio of the mean fluorescence intensity of the proximal regions relative to those distal to the surgical site was used to indicate the uptake of FITC-dextran.

Whole-mount staining

For three-dimensional whole-mount staining, mouse tails were cut into 3-mm pieces after fixation with 4% paraformaldehyde (Leagene, China). Samples were incubated with BODIPY dye (5 μM, Molecular Probes, USA) and Hoechst 33258 (5 μg/ml, Beyotime, China) for 20 minutes at room temperature. After washing 3 times with PBS, the samples were imaged using a laser confocal microscope (Nikon A1, Japan).

Histological examination

Harvested mouse tails were fixed with 4% paraformaldehyde for 24~48 hours and then decalcified for 7~10 days at 37°C with 10% EDTA.

Samples were then embedded in paraffin and sectioned for hematoxylin/eosin staining (H&E) and Masson trichrome staining. ImageJ was used for adipocyte diameter measurement and collagen quantification.

Immunofluorescent staining

Briefly, tails were fixed with 4% paraformaldehyde for 24~48 hours. Full-thickness skin was stripped and dehydrated with 30% sucrose solution for 48 hours. Frozen tissue specimens were sliced into 6-μm sections after being embedded with Optimal Cutting Temperature (OCT) compound (Sakura, USA).

After antigen retrieval with citrate repair solution (ZSGB-Bio, China) and blocking nonspecific binding with sheep serum (ZSGB-Bio, China), the samples were incubated with the following primary antibodies overnight at 4°C: anti-lymphatic vessel endothelial hyaluronan receptor-1 (LYVE-1) (1:500, polyclonal, Abcam, UK) and anti-CD4 (1:100, clone EPR19514, Abcam, UK). Alexa Fluor 488-conjugated goat anti-rabbit IgG (Abcam, UK) and Alexa Fluor® 594-conjugated goat anti-rabbit IgG (Abcam, UK) were used as the secondary antibodies. Nuclei were stained with 4, 6-diamino-2-phenylindole (DAPI).

Statistical analysis

Data were analyzed using 2-tailed Student's t tests with GraphPad Prism software (GraphPad Software, Inc., San Diego, CA). Comparison values of $P \leq 0.05$ were considered significant.

Results

Specific lymphatic reflux blockade effect of the mouse tail lymphedema model

We generated a mouse tail lymphedema model by excising a 2-mm-wide skin section of the mouse tail and disconnecting the collecting lymphatic vessels (**Figure 1A-C**). The model creates a pathological change that mimics the obstruction of lymphatic drainage in patients. ICG and FITC-dextran were injected subcutaneously 2 weeks after surgery to study whether lymphatic drainage was effectively blocked. Because of their large molecular weights, these two fluorescent substances can be absorbed only by lymphatic vessels but not blood vessels after subcutaneous injection, and thus, they can respond to lymphatic reflux. Both detection methods showed that the macromolecular fluorescent substance was concentrated distal to the surgical incision, and no fluorescence was observed in the proximal site (**Figure 1D** and **1E**). These results demonstrate the exact effect of lymphatic reflux blockade.

Changes in mouse tail edema after surgery

Given that changes in postoperative edema and the self-limiting time directly determine the experimental plan after intervention, it is necessary to observe a model of swelling. To study this determinant, we measured the tail diameters at the -1 cm, +0.5 cm and +1 cm sites and the tail volumes every week and compared these values with those before surgery (the measurement site is labeled as shown in **Figure 1A**). Tail swelling peaked at the third week and decreased slowly until it entered a plateau phase at the sixth week. In addition, there was no significant change in the diameter of the tail at the -1 cm site (**Figure 2A** and **2B**), which indicates that the surgery had no effect on the proximal tail. H&E staining showed changes in the tail diameter more intuitively (**Figure 2C**).

Subcutaneous adipose tissue thickening in the mouse tail model

As adipose tissue hyperplasia is an important pathologic change in lymphedema [13], we aimed to detect subcutaneous adipose thickness. H&E staining revealed thickening of the subcutaneous tissue after surgery (**Figure 2C** and **2D**). To detect adipose tissue more accurately, we applied whole-mount staining and stained oil droplets with BODIPY. The results showed that cells colored by BODIPY were adipocytes, except for sebaceous gland staining (**Figure 2D**). As shown in the results, the normal tail has a thin layer of adipose tissue, mostly a monolayer or double layer of adipocytes, with an average thickness of 52 μm. This layer was significantly thickened at 3 weeks and then decreased at 9 weeks after surgery, with an average thickness of 440 μm and 270 μm, respectively (**Figure 2E** and **2F**). These results suggest that the change in subcutaneous adipose thickness in the mouse tail is consistent with the degree of postsurgical mouse edema, volume, and diameter changes.

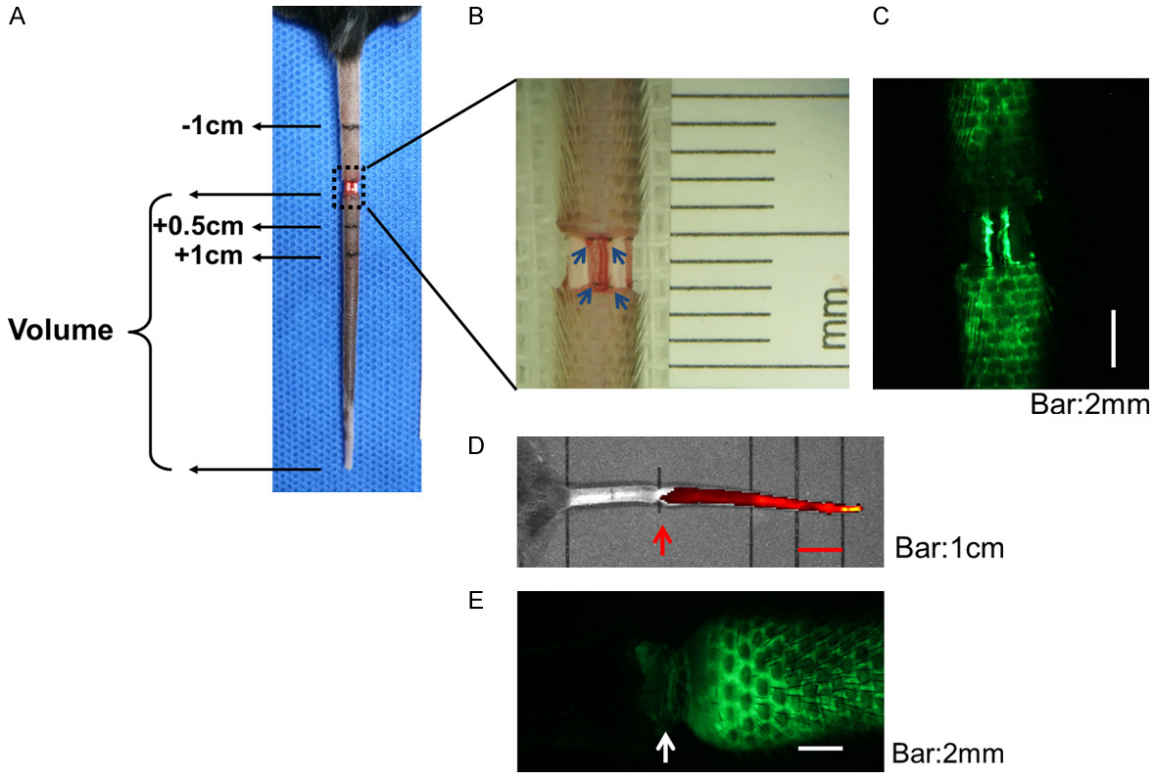

Figure 1. Lymphatic edema mouse tail model surgery and postoperative lymphatic drainage examination. (A) Surgical and measurement sites of the mouse tail. (B) Representative images of the surgical site under the microscope. (C) FITC-dextran was injected subcutaneously at the distal aspect of the incision after skin circumcision, and collecting lymphatic vessels on both sides of the lateral vein were observed under a fluorescence microscope. (D, E) Lymphatic vessel transport evaluation using ICG (D) and FITC-dextran (E) 2 weeks after surgery (the arrow points to the surgical incision).

Gradually worsening tissue fibrosis after surgery

To study collagen deposition in subcutaneous tissue, we performed Masson staining, which stained the collagen fibers blue and the muscle fibers red. The results showed that collagen fibers in the dermis of the skin were arranged densely and orderly, and the subcutaneous tissue was scattered throughout the blue-stained fiber region. Lymphedema in subcutaneous tissues was characterized by a dense deposition of collagen fibers and a gradually increasing percentage of fibrotic areas, showing the development of fibrosis subcutaneously in the tails after surgery (**Figure 3C** and **3D**). The percentage of the fibrotic area in the normal subcutaneous tissue was too small to analyze statistically.

Gradually increasing CD4$^+$ T lymphocyte infiltration

The infiltration of local CD4$^+$ T lymphocytes was detected by immunofluorescence staining, and statistical analysis was performed. CD4$^+$ T cells infiltrated the skin 1 week after surgery, and increased rapidly, with a large number of CD4$^+$ T cells infiltrating 9 weeks after surgery (**Figure 3A** and **3B**). Although swelling of the tail peaked at 3 weeks after surgery and entered the plateau at 6 weeks, the lymphedema did not fully resolve as the inflammatory reaction continued. Eventually, the number of CD4$^+$ T cells was significantly reduced at 14 weeks after surgery.

Lymphatic vessel expansion and lymphatic reflow reconstruction during lymphedema development

We next evaluated lymphatic vessels using immunofluorescence staining for LYVE-1, which is a lymphatic vessel marker. The results showed profound enlargement of lymphatic vessels after surgery (**Figure 4A**). The lymphatic vessel cross-sectional area in the tail skin increased 1 week after surgery and peaked at 3 weeks, showing significant expansion. In

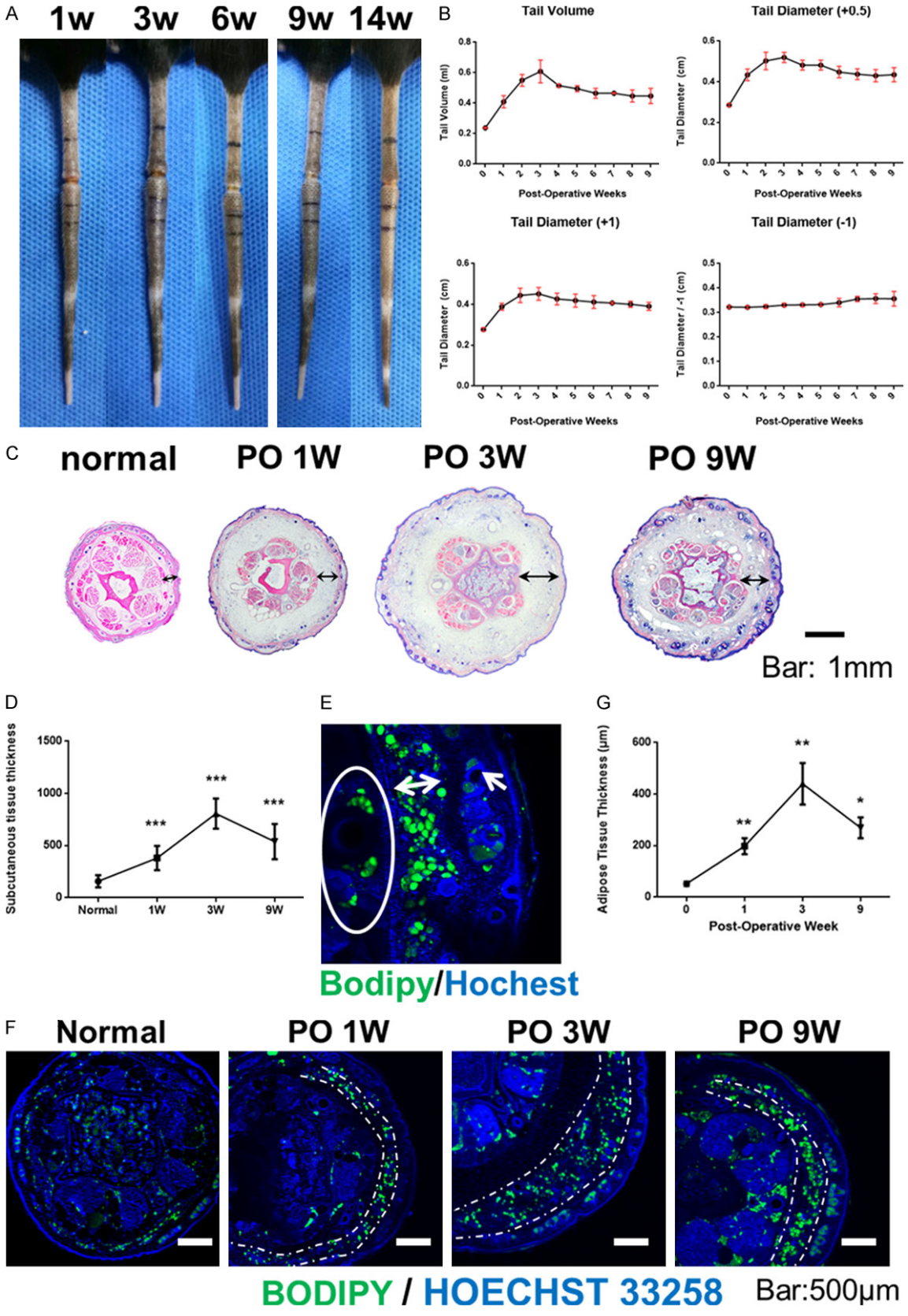

Figure 2. Changes in edema and subcutaneous fat thickening in mouse tail lymphedema models. A. Representative images of the mouse tail at 1, 3, 6, and 9 weeks after surgery. B. Tail volume and diameter were measured before

and after surgery. C. Histologic sections of the mouse tails were stained with H&E. Subcutaneous tissue is indicated by the arrow. D. Subcutaneous tissue thickness. E. Whole-mount staining of the mouse tail showing intact lipid droplets. Sebaceous gland staining is indicated by the arrow, adipose tissue around the muscle is shown within the circle, and the double arrow indicates the subcutaneous adipose tissue layer. F. Whole-mount staining of a normal mouse tail and tail models at 1, 3, and 9 weeks after surgery showing the thickness of the subcutaneous adipose layer. G. A graph of the subcutaneous adipose thickness (each set of data was compared to the previous week's values). Statistical analysis was performed with Student's t-test. The results were considered significant at $P<0.05$. $^{*}P<0.05$, $^{**}P<0.01$, and $^{***}P<0.001$.

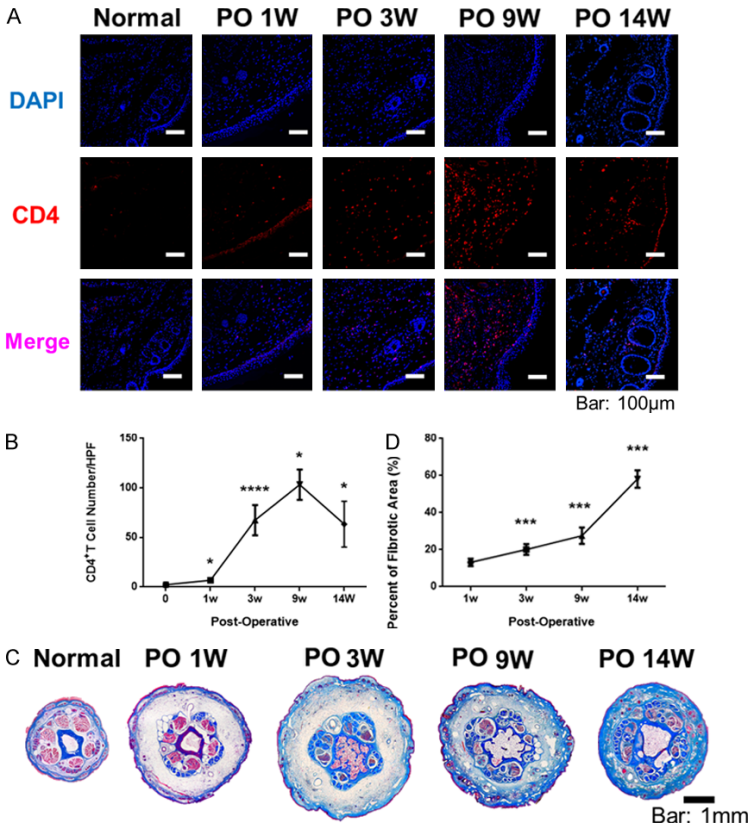

Figure 3. $CD4^{+}$ T lymphocyte infiltration and subcutaneous tissue fibrosis in the lymphedema tail model. A. $CD4^{+}$ T lymphocytes were stained for immunofluorescence in the normal tail and at 1, 3, and 9 weeks after surgery. B. The number of $CD4^{+}$ T lymphocytes per HPF was measured. C. Masson staining was used to detect collagen fiber deposition in the subcutaneous tissue. D. Graph of the area ratio of collagen fibers. Collagen fiber deposition is represented by the area ratio measured by ImageJ. Statistical analysis was performed with Student's t-test. The results were considered significant at $P<0.05$. $^{*}P<0.05$, $^{**}P<0.01$, and $^{***}P<0.001$.

addition, we counted the number of lymphatic vessels per high-power field (HPF) of view; this number increased significantly at 3 weeks and continued to increase thereafter (**Figure 4A-C**).

Lymphatic reflux was measured by the subcutaneous injection of FITC-dextran and photographed by fluorescence microscopy. Fluorescent dyes were not observed through the surgical incision at 6 weeks after surgery. Eight weeks after surgery, no fluorescent dye was observed passing through the surgical incision after 15 minutes of injection; however, the dye was observed after 45 minutes. Fluorescent tracers in the proximal portion of the tail demonstrated markedly increased transport of the fluorescent dye at 14 weeks. In addition, the perfused honeycomb pattern of lymphatic capillaries was clearly displayed at 14 weeks after surgery (**Figure 4D**).

Discussion

It has been reported that the mouse tail model has a low success rate (65%) and is prone to necrosis after surgery [3]. However, we found that attention to the following details in the modeling process can effectively avoid necrosis. First, blood vessels must be protected from damage during the operation. We operated near the surgical margin when ligating and disconnecting deep lymphatic vessels and tried to protect the vascular envelope and connective tissue around it instead of skeletonizing the blood vessels. Second, a 3M Tegaderm dressing was wrapped around the incision immediately after surgery. In addition to preventing infection, the dressing exerted a local moisturizing effect to prevent postoperative vascular injury caused by dryness. Third, only 2-3 mice were kept in each cage after the operation to avoid the tail-to-tail impact caused by frequent movement. Finally, when we handled the mice, we grasped the site proximal to the surgical incision rather than the distal site. This technique effectively avoided artificial damage

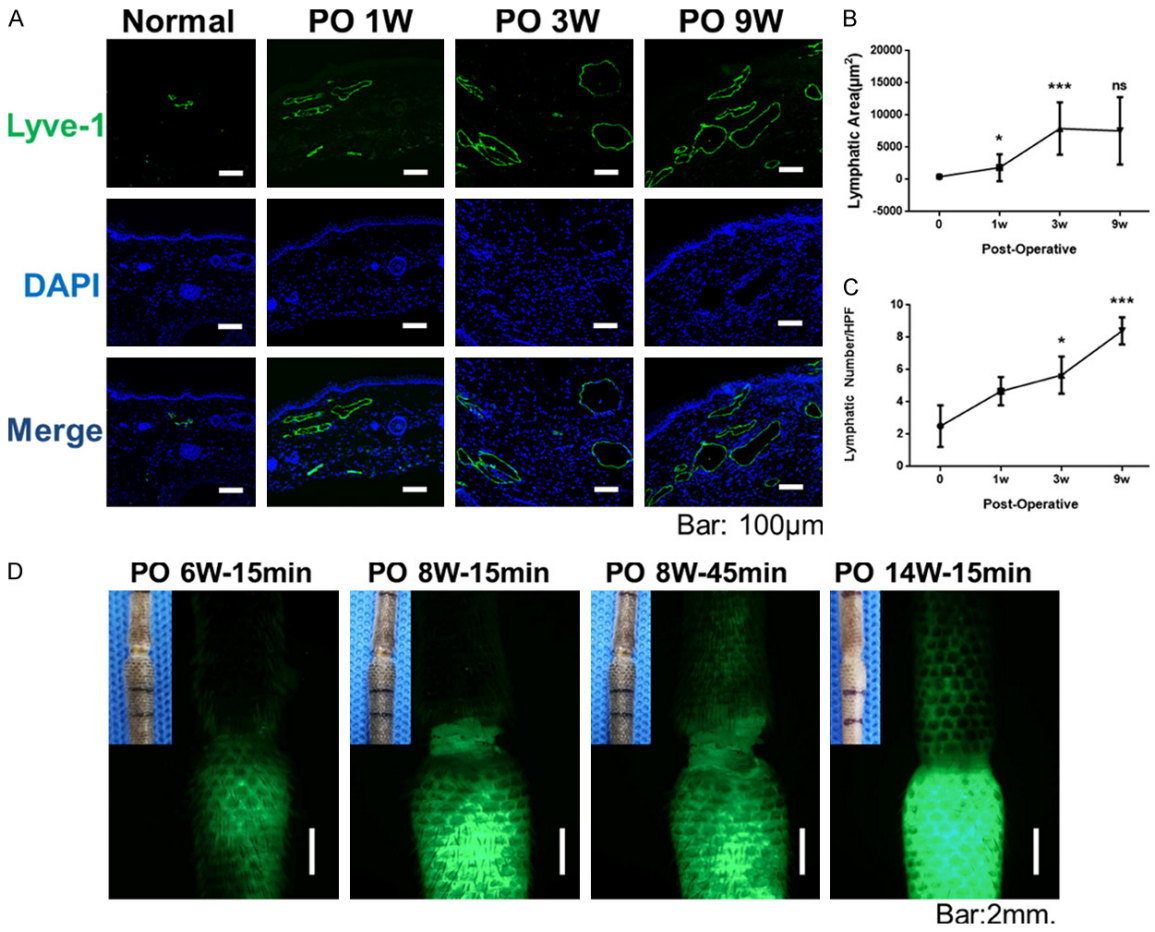

Figure 4. Lymphatic vessel regeneration and lymphatic drainage in the mouse tail lymphedema model. A. Subcutaneous LYVE-1$^+$ lymphatic vessels were detected by immunofluorescence staining. B. Statistical analysis of the lymphatic cross-sectional area at specified times. C. Statistical analysis of the number of lymphatic vessels per HPF. D. Lymphatic reflux was detected by the subcutaneous injection of FITC-dextran and photographed by fluorescence microscopy after 15 minutes and 45 minutes. Statistical analysis was performed with Student's t-test. The results were considered significant at $P<0.05$. *$P<0.05$, **$P<0.01$, and ***$P<0.001$.

caused by violent movements, such as lifting the tail. The overall success rate of the tail model was more than 80% in our study, which was significantly higher than that reported in a previous study [3].

After demonstrating the exact effect of lymphatic reflux blockade during surgery, we measured the diameters and volumes of the tails. The results showed that swelling of the tail entered a plateau after 6 weeks, which indicates that the swelling caused by surgery was relieved spontaneously. This result was consistent with those from previous studies [2, 14]. The spontaneous resolution of swelling exposed an important limitation of the tail model (i.e., it could not closely simulate clinical chronic lymphedema). Secondary lymphedema disease is a chronic disease that develops months or even years after initial injury and is a progressive disease once activated. Therefore, experiments are required at an early stage if we expect to visually observe changes in tail edema when we use this model to study lymphedema.

As adipose hyperplasia is an important pathological change in lymphedema, the thickness of adipose tissue detected by Oil Red O staining is used as an important indicator for assessing the severity of lymphedema in some studies [15, 16]. However, our study showed that Oil Red O staining is difficult to implement, as reflected by nonspecific coloration, which may

be caused by broken lipid droplets. Therefore, we used whole-mount BODIPY staining to display lipid droplets. We showed that the thickness of the subcutaneous adipose tissue was highly similar to that of the tail volume and diameter (i.e., there was significant thickening at 1 week after surgery, a significant increase at 3 weeks, and a decrease at 9 weeks).

In addition to adipose hyperplasia, fibrosis is another important pathologic change in lymphedema. Researchers believe that tissue fibrosis can limit adipose hyperplasia [17]. Therefore, we believe that the decrease in subcutaneous adipose thickness between 3 weeks and 9 weeks after surgery was caused by progressively increased fibrosis. In addition, the fibers around muscles and between the muscle fibers increased after modeling. This fibrous exudation may have been caused by local inflammatory irritation.

Lymph fluid retention resulted in marked inflammation in the local tissue, as reflected by immune cell infiltration and inflammatory factors. Garcia Nores [15] proposed that $CD4^+$ T cells in skin-draining lymph nodes are activated following lymph fluid retention and are then released and migrate to the skin, promoting the development of lymphedema. Considering the important role of $CD4^+$ T lymphocytes in lymphedema, we examined the infiltration of $CD4^+$ T lymphocytes after modeling. We showed that lymphatic stasis led to a gradual increase in $CD4^+$ T cell infiltration. This result suggests that a local inflammatory response still exists at 9 weeks after surgery. Notably, the lymphedema did not resolve, although swelling of the tail plateaued at 6 weeks postoperatively.

Lymphatic drainage is blocked in lymphedema, leading to the expansion of capillary lymphatic vessels in the skin. Moreover, the number of lymphatic vessels per HPF was significantly increased, and these vessels were considered to be newly generated lymphatic vessels. At 1 week after surgery, there was no increase in the number of lymphatic vessels per HPF, although the area of the lymphatic vessels was expanded. Studies have reported that the peak of VEGF-C expression lags behind LEC proliferation and vessel hyperplasia peaks [18]. Therefore, we believe that the retention of lymph causes lymphatic vessel expansion followed by the generation of lymphatic vessels.

A previous study indicated a progressive loss of function of lymphatic vessels during lymphedema development [14], and the excessive generation of immature lymphatic vessels is essential for initial edema development and the later development of lymphedema pathology [9]. We showed here that maximal swelling was noted shortly after surgery and resolved spontaneously over time in the tail model. How does edema resolve in cases where lymphatic vessel function continues to deteriorate? We hypothesized that with the gradual healing of the surgical incision, the newly formed lymphatic vessels could subsequently promote lymphatic reflux and thus improve the edema. We showed here that reflux is not established until 8 weeks after surgery. The honeycomb lymphatic capillary pattern was clearly observed at 14 weeks, indicating increased perfusion of the lymphatic capillary vessels [14].

In this study, we mainly explored details in modeling methods and model characteristics of the mouse tail model, including swelling of the tail, thickness of the subcutaneous adipose tissue, fibrosis, $CD4^+$ T cell infiltration, number and morphology of the lymphatic vessels, and lymphatic drainage. In fact, these pathologic changes are interrelated. Lymphatic stagnation leads to local inflammatory conditions, which in turn lead to pathologic changes characterized by adipose tissue hyperplasia and fibrosis [13, 16]. Adipose tissue is considered an important endocrine organ [19]. Studies have found that adipose tissue in obese patients can promote the abnormal recruitment and inflammatory responses of immune cells through multiple pathways [20-23]. For example, hypertrophic adipocytes secrete a variety of cytokines, such as monocyte TNF-α, IL-6, IL-8, and leptin [24, 25]. A variety of immune cells and inflammatory factors are involved in the regulation of fibrosis in lymphedema. Among these are factors that may play a profibrotic role in lymphedema, including TGF-β1 [26-32], PDGF [33, 34], IL-6 [35-39], IL-4, and IL-13 [4, 40-42]. In addition, exocrine factors, including IL-10 [43], adiponectin [44-47], and PPAR-γ [48], may exert antifibrosis effects. Based on these findings, we speculated that hyperplastic adipose tissue caused by inflammation in turn participates in the local inflammatory response and fibrosis. In turn, tissue fibrosis can limit adipose hyperpla-

sia. Studies have found that fibrosis occurs not only in subcutaneous tissue [13] but also in the wall of lymphatic vessels [49], and this fibrosis severely affects the function of lymphatic vessels and aggravates lymphedema [16, 49, 50].

These findings are of great significance for the application of the mouse tail model in research. As we show here, tissue fibrosis continued to deteriorate, although the tail swelling, subcutaneous adipose hyperplasia, and $CD4^+$ T cell infiltration were alleviated, and lymphatic reflux was established over time. If the study period is more than 9 weeks, then tissue fibrosis can be used as an evaluation index instead of characteristic changes, such as tail swelling. In addition, by mastering the changes after modeling, such as the time necessary to establish lymphatic reflow, we can grasp the detection time and the reasonable comparison index more accurately when applying the model. Our results demonstrate the irreversibility of fibrosis, suggesting an important role for fibrosis in the later stages of lymphedema, and the importance of treating lymphedema by preventing the development of fibrosis.

Acknowledgements

The animal experiments in this study were approved by the Animal Ethics Committee of Beijing Shijitan Hospital affiliated with Capital Medical University.

Disclosure of conflict of interest

None.

Address correspondence to: Lei Cui, Department of Central Laboratory, Beijing Shijitan Hospital, Capital Medical University, Beijing 100038, China. Tel: +86-18515272537; E-mail: sjtbeijing@163.com

References

[1] Executive Committee. The diagnosis and treatment of peripheral lymphedema: 2016 consensus document of the international society of lymphology. Lymphology 2016; 49: 170-84.

[2] Hadrian R and Palmes D. Animal models of secondary lymphedema: new approaches in the search for therapeutic options. Lymphat Res Biol 2017; 15: 2-16.

[3] Jun H, Lee JY, Kim JH, Noh M, Kwon TW, Cho YP and Yoon YS. Modified mouse models of chronic secondary lymphedema: tail and hind limb models. Ann Vasc Surg 2017; 43: 288-295.

[4] Avraham T, Zampell JC, Yan A, Elhadad S, Weitman ES, Rockson SG, Bromberg J and Mehrara BJ. Th2 differentiation is necessary for soft tissue fibrosis and lymphatic dysfunction resulting from lymphedema. FASEB J 2013; 27: 1114-26.

[5] Hwang JH, Kim IG, Lee JY, Piao S, Lee DS, Lee TS, Ra JC and Lee JY. Therapeutic lymphangiogenesis using stem cell and VEGF-C hydrogel. Biomaterials 2011; 32: 4415-23.

[6] Yoshida S, Hamuy R, Hamada Y, Yoshimoto H, Hirano A and Akita S. Adipose-derived stem cell transplantation for therapeutic lymphangiogenesis in a mouse secondary lymphedema model. Regen Med 2015; 10: 549-62.

[7] Kataru RP, Jung K, Jang C, Yang H, Schwendener RA, Baik JE, Han SH, Alitalo K and Koh GY. Critical role of CD11b+ macrophages and VEGF in inflammatory lymphangiogenesis, antigen clearance, and inflammation resolution. Blood 2009; 113: 5650-9.

[8] García Nores GD, Ly CL, Savetsky IL, Kataru RP, Ghanta S, Hespe GE, Rockson SG and Mehrara BJ. Regulatory T cells mediate local immunosuppression in lymphedema. J Invest Dermatol 2018; 138: 325-335.

[9] Ogata F, Fujiu K, Matsumoto S, Nakayama Y, Shibata M, Oike Y, Koshima I, Watabe T, Nagai R and Manabe I. Excess lymphangiogenesis cooperatively induced by macrophages and CD4(+) T cells drives the pathogenesis of lymphedema. J Invest Dermatol 2016; 136: 706-714.

[10] Gardenier JC, Hespe GE, Kataru RP, Savetsky IL, Torrisi JS, Nores GDG, Dayan JJ, Chang D, Zampell J, Martínez-Corral I, Ortega S and Mehrara BJ. Diphtheria toxin-mediated ablation of lymphatic endothelial cells results in progressive lymphedema. JCI Insight 2016; 1: e84095.

[11] Yang CY, Nguyen DH, Wu CW, Fang YH, Chao KT, Patel KM and Cheng MH. Developing a lower limb lymphedema animal model with combined lymphadenectomy and low-dose radiation. Plast Reconstr Surg Glob Open 2014; 2: e121.

[12] Grada AA and Phillips TJ. Lymphedema: pathophysiology and clinical manifestations. J Am Acad Dermatol 2017; 77: 1009-1020.

[13] Tashiro K, Feng J, Wu SH, Mashiko T, Kanayama K, Narushima M, Uda H, Miyamoto S, Koshima I and Yoshimura K. Pathological changes of adipose tissue in secondary lymphoedema. Br J Dermatol 2017; 177: 158-167.

[14] Gousopoulos E, Proulx ST, Scholl J, Uecker M and Detmar M. Prominent lymphatic vessel hy-

perplasia with progressive dysfunction and distinct immune cell infiltration in lymphedema. Am J Pathol 2016; 186: 2193-2203.
[15] García Nores GD, Ly CL, Cuzzone DA, Kataru RP, Hespe GE, Torrisi JS, Huang JJ, Gardenier JC, Savetsky IL, Nitti MD, Yu JZ, Rehal S and Mehrara BJ. CD4(+) T cells are activated in regional lymph nodes and migrate to skin to initiate lymphedema. Nat Commun 2018; 9: 1970.
[16] Zampell JC, Aschen S, Weitman ES, Yan A, Elhadad S, De Brot M and Mehrara BJ. Regulation of adipogenesis by lymphatic fluid stasis: part I. Adipogenesis, fibrosis, and inflammation. Plast Reconstr Surg 2012; 129: 825-34.
[17] Divoux A, Tordjman J, Lacasa D, Veyrie N, Hugol D, Aissat A, Basdevant A, Guerre-Millo M, Poitou C, Zucker JD, Bedossa P and Clément K. Fibrosis in human adipose tissue: composition, distribution, and link with lipid metabolism and fat mass loss. Diabetes 2010; 59: 2817-25.
[18] Rutkowski JM, Moya M, Johannes J, Goldman J and Swartz MA. Secondary lymphedema in the mouse tail: lymphatic hyperplasia, VEGF-C upregulation, and the protective role of MMP-9. Microvasc Res 2006; 72: 161-71.
[19] Schäffler A and Schölmerich J. Innate immunity and adipose tissue biology. Trends Immunol 2010; 31: 228-35.
[20] Osborn O and Olefsky JM. The cellular and signaling networks linking the immune system and metabolism in disease. Nat Med 2012; 18: 363-74.
[21] Exley MA, Hand L, O'Shea D and Lynch L. Interplay between the immune system and adipose tissue in obesity. J Endocrinol 2014; 223: R41-8.
[22] Deng T, Lyon CJ, Minze LJ, Lin J, Zou J, Liu JZ, Ren Y, Yin Z, Hamilton DJ, Reardon PR, Sherman V, Wang HY, Phillips KJ, Webb P, Wong ST, Wang RF and Hsueh WA. Class II major histocompatibility complex plays an essential role in obesity-induced adipose inflammation. Cell Metab 2013; 17: 411-22.
[23] Xiao L, Yang X, Lin Y, Li S, Jiang J, Qian S, Tang Q, He R and Li X. Large adipocytes function as antigen-presenting cells to activate CD4(+) T cells via upregulating MHCII in obesity. Int J Obes (Lond) 2016; 40: 112-20.
[24] Hosogai N, Fukuhara A, Oshima K, Miyata Y, Tanaka S, Segawa K, Furukawa S, Tochino Y, Komuro R, Matsuda M and Shimomura I. Adipose tissue hypoxia in obesity and its impact on adipocytokine dysregulation. Diabetes 2007; 56: 901-11.
[25] Sun K, Kusminski CM and Scherer PE. Adipose tissue remodeling and obesity. J Clin Invest 2011; 121: 2094-101.
[26] Bataller R and Brenner DA. Liver fibrosis. J Clin Invest 2005; 115: 209-18.
[27] Yu G, Tzouvelekis A, Wang R, Herazo-Maya JD, Ibarra GH, Srivastava A, de Castro JPW, Deluliis G, Ahangari F, Woolard T, Aurelien N, Arrojo E Drigo R, Gan Y, Graham M, Liu X, Homer RJ, Scanlan TS, Mannam P, Lee PJ, Herzog EL, Bianco AC and Kaminski N. Thyroid hormone inhibits lung fibrosis in mice by improving epithelial mitochondrial function. Nat Med 2018; 24: 39-49.
[28] Larson-Casey JL, Deshane JS, Ryan AJ, Thannickal VJ and Carter AB. Macrophage Akt1 kinase-mediated mitophagy modulates apoptosis resistance and pulmonary fibrosis. Immunity 2016; 44: 582-596.
[29] Guo Y, Gupte M, Umbarkar P, Singh AP, Sui JY, Force T and Lal H. Entanglement of GSK-3beta, beta-catenin and TGF-beta1 signaling network to regulate myocardial fibrosis. J Mol Cell Cardiol 2017; 110: 109-120.
[30] Higgins DF, Ewart LM, Masterson E, Tennant S, Grebnev G, Prunotto M, Pomposiello S, Conde-Knape K, Martin FM and Godson C. BMP7-induced-Pten inhibits Akt and prevents renal fibrosis. Biochim Biophys Acta Mol Basis Dis 2017; 1863: 3095-3104.
[31] Mitra A, Luna JI, Marusina AI, Merleev A, Kundu-Raychaudhuri S, Fiorentino D, Raychaudhuri SP and Maverakis E. Dual mTOR inhibition is required to prevent TGF-beta-mediated fibrosis: implications for scleroderma. J Invest Dermatol 2015; 135: 2873-2876.
[32] Martin M, Lefaix J and Delanian S. TGF-beta1 and radiation fibrosis: a master switch and a specific therapeutic target? Int J Radiat Oncol Biol Phys 2000; 47: 277-90.
[33] Borkham-Kamphorst E and Weiskirchen R. The PDGF system and its antagonists in liver fibrosis. Cytokine Growth Factor Rev 2016; 28: 53-61.
[34] Shah R, Reyes-Gordillo K, Arellanes-Robledo J, Lechuga CG, Hernández-Nazara Z, Cotty A, Rojkind M and Lakshman MR. TGF-beta1 up-regulates the expression of PDGF-beta receptor mRNA and induces a delayed PI3K-, AKT-, and p70(S6K)-dependent proliferative response in activated hepatic stellate cells. Alcohol Clin Exp Res 2013; 37: 1838-48.
[35] Fielding CA, Jones GW, McLoughlin RM, McLeod L, Hammond VJ, Uceda J, Williams AS, Lambie M, Foster TL, Liao CT, Rice CM, Greenhill CJ, Colmont CS, Hams E, Coles B, Kift-Morgan A, Newton Z, Craig KJ, Williams JD, Williams GT, Davies SJ, Humphreys IR, O'Donnell VB, Taylor PR, Jenkins BJ, Topley N and Jones SA. Interleukin-6 signaling drives fibrosis in unresolved inflammation. Immunity 2014; 40: 40-50.

[36] O'Reilly S, Ciechomska M, Cant R and van Laar JM. Interleukin-6 (IL-6) trans signaling drives a STAT3-dependent pathway that leads to hyperactive transforming growth factor-beta (TGF-beta) signaling promoting SMAD3 activation and fibrosis via Gremlin protein. J Biol Chem 2014; 289: 9952-60.

[37] Kechagia JZ, Ezra DG, Burton MJ and Bailly M. Fibroblasts profiling in scarring trachoma identifies IL-6 as a functional component of a fibroblast-macrophage pro-fibrotic and pro-inflammatory feedback loop. Sci Rep 2016; 6: 28261.

[38] Chen R, Sun Y, Cui X, Ji Z, Kong X, Wu S, Huang Q, Dai X, Zhang S, Ma L and Jiang L. Autophagy promotes aortic adventitial fibrosis via the IL-6/Jak1 signaling pathway in Takayasu's arteritis. J Autoimmun 2019; 99: 39-47.

[39] Hu L, Yu Y, Huang H, Fan H, Hu L, Yin C, Li K, Fulton DJ and Chen F. Epigenetic regulation of interleukin 6 by histone acetylation in macrophages and its role in paraquat-induced pulmonary fibrosis. Front Immunol 2017; 7: 696.

[40] Oriente A, Fedarko NS, Pacocha SE, Huang SK, Lichtenstein LM and Essayan DM. Interleukin-13 modulates collagen homeostasis in human skin and keloid fibroblasts. J Pharmacol Exp Ther 2000; 292: 988-94.

[41] Chiaramonte MG, Donaldson DD, Cheever AW and Wynn TA. An IL-13 inhibitor blocks the development of hepatic fibrosis during a T-helper type 2-dominated inflammatory response. J Clin Invest 1999; 104: 777-85.

[42] Murray LA, Argentieri RL, Farrell FX, Bracht M, Sheng H, Whitaker B, Beck H, Tsui P, Cochlin K, Evanoff HL, Hogaboam CM and Das AM. Hyper-responsiveness of IPF/UIP fibroblasts: interplay between TGFbeta1, IL-13 and CCL2. Int J Biochem Cell Biol 2008; 40: 2174-82.

[43] Zhang LJ, Zheng WD, Chen YX, Huang YH, Chen ZX, Zhang SJ, Shi MN and Wang XZ. Antifibrotic effects of interleukin-10 on experimental hepatic fibrosis. Hepatogastroenterology 2007; 54: 2092-8.

[44] Fang F, Liu L, Yang Y, Tamaki Z, Wei J, Marangoni RG, Bhattacharyya S, Summer RS, Ye B and Varga J. The adipokine adiponectin has potent anti-fibrotic effects mediated via adenosine monophosphate-activated protein kinase: novel target for fibrosis therapy. Arthritis Res Ther 2012; 14: R229.

[45] Handy JA, Fu PP, Kumar P, Mells JE, Sharma S, Saxena NK and Anania FA. Adiponectin inhibits leptin signalling via multiple mechanisms to exert protective effects against hepatic fibrosis. Biochem J 2011; 440: 385-95.

[46] Mishra R, Cool BL, Laderoute KR, Foretz M, Viollet B and Simonson MS. AMP-activated protein kinase inhibits transforming growth factor-beta-induced Smad3-dependent transcription and myofibroblast transdifferentiation. J Biol Chem 2008; 283: 10461-9.

[47] Scherer PE, Williams S, Fogliano M, Baldini G and Lodish HF. A novel serum protein similar to C1q, produced exclusively in adipocytes. J Biol Chem 1995; 270: 26746-9.

[48] Wei J, Zhu H, Komura K, Lord G, Tomcik M, Wang W, Doniparthi S, Tamaki Z, Hinchcliff M, Distler JH and Varga J. A synthetic PPAR-gamma agonist triterpenoid ameliorates experimental fibrosis: PPAR-gamma-independent suppression of fibrotic responses. Ann Rheum Dis 2014; 73: 446-54.

[49] Avraham T, Clavin NW, Daluvoy SV, Fernandez J, Soares MA, Cordeiro AP and Mehrara BJ. Fibrosis is a key inhibitor of lymphatic regeneration. Plast Reconstr Surg 2009; 124: 438-50.

[50] Lynch LL, Mendez U, Waller AB, Gillette AA, Guillory RJ 2nd and Goldman J. Fibrosis worsens chronic lymphedema in rodent tissues. Am J Physiol Heart Circ Physiol 2015; 308: H1229-36.